



Physical Chemistry for Medical Applications
European Meeting on Physical Organic Chemistry
Wroclaw - Wojcieszów, 01-05.06.2026

Plenary lectures and oral presentations



Prof. dr hab. Małgorzata Barańska

Challenges in spectroscopic
imaging of cells: an analytical and
physical chemistry perspective





Dr hab. Sylwester Mazurek

Discriminant analysis of
seminal plasma samples
using FTIR-ATR spectroscopy

Dr Barbara Zupančič

Identifying diabetes-related
biochemical changes in human
tissues using infrared spectroscopy





**Dr hab. Zbigniew Galewski,
Prof. UWr**

Liquid crystals in medical
applications

Dr Amanda Bartkowiak

SGLT 2 inhibition improves red blood cell oxygenation and elasticity: another positive effect of flozin therapy





Dr Iwona Płowaś-Korus

Osmolytes in humans -
biological significance and
clinical implications

**Chemistry for Medical
Applications**

01-05.06.2026

Prof. dr hab. Kazimierz Orzechowski

Dielectric methods in assessing the
cleanliness of surgical margins in breast
cancer



Dr hab. Andrzej Teisseyre

The inhibitory effects of selected flavonoids
on the activity of voltage-gated potassium
channels Kv1.3





Dr Marta Gordel-Wójcik

Ultrafast excited-state dynamics
in trimethoxysilylazachalcone-
functionalized colloidal gold
nanoshells

Physical

Dr Justyna Krupa

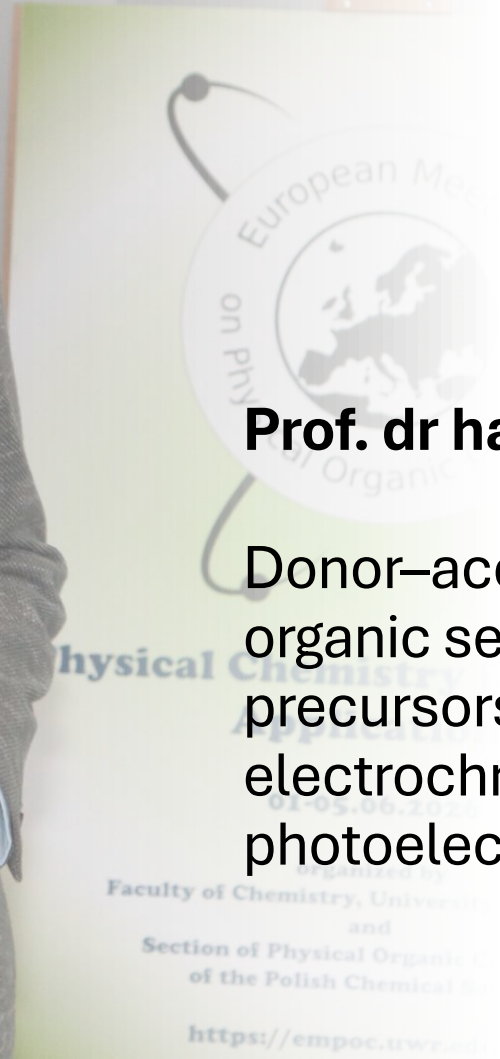
UV-induced chemistry in interstellar ice analogues: from simple molecules to complex systems



Prof. dr hab. Teobald Kupka

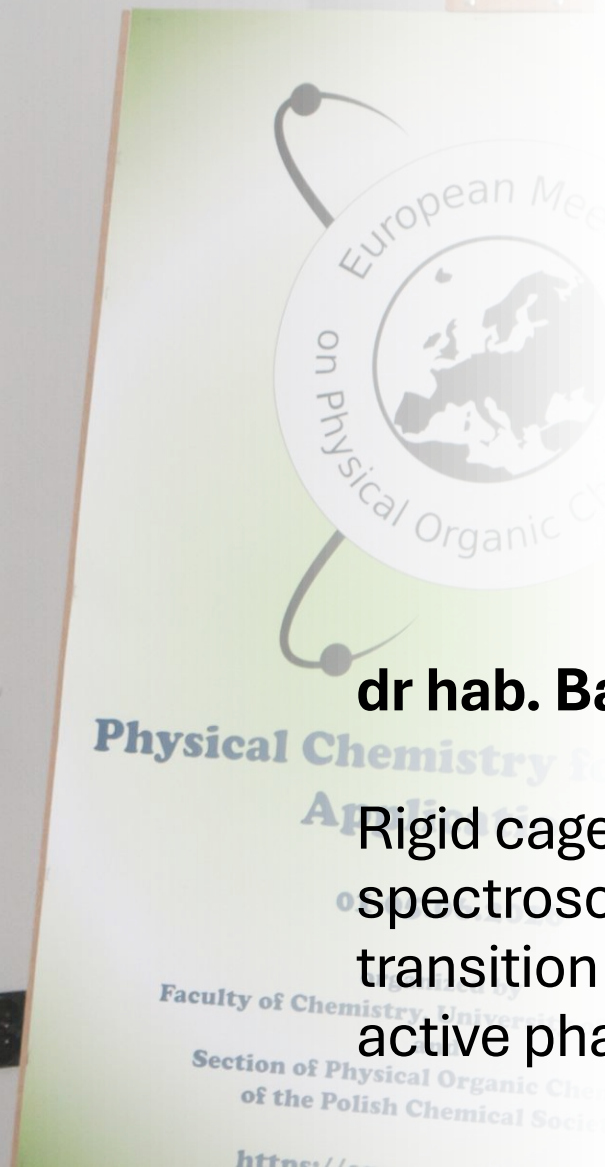
Toward accurate NMR shieldings in
fluoromethanes





Prof. dr hab. Adam Proń

Donor–acceptor macromolecular organic semiconductors as precursors of novel electronic, electrochromic, and photoelectrocatalytic materials



dr hab. Barbara Hachuła, prof. UŚ

Rigid cage, variable nature:
spectroscopic study of phase
transition in adamantane-based
active pharmaceutical ingredients

Prof. Poul Erik Hansen

Drugs, natural products and
hydrogen bonding (online lecture)



Dr hab. inż. Rafał Szabla

Machine learning in RNA atomistic
simulations



Dr Michał Pocheć

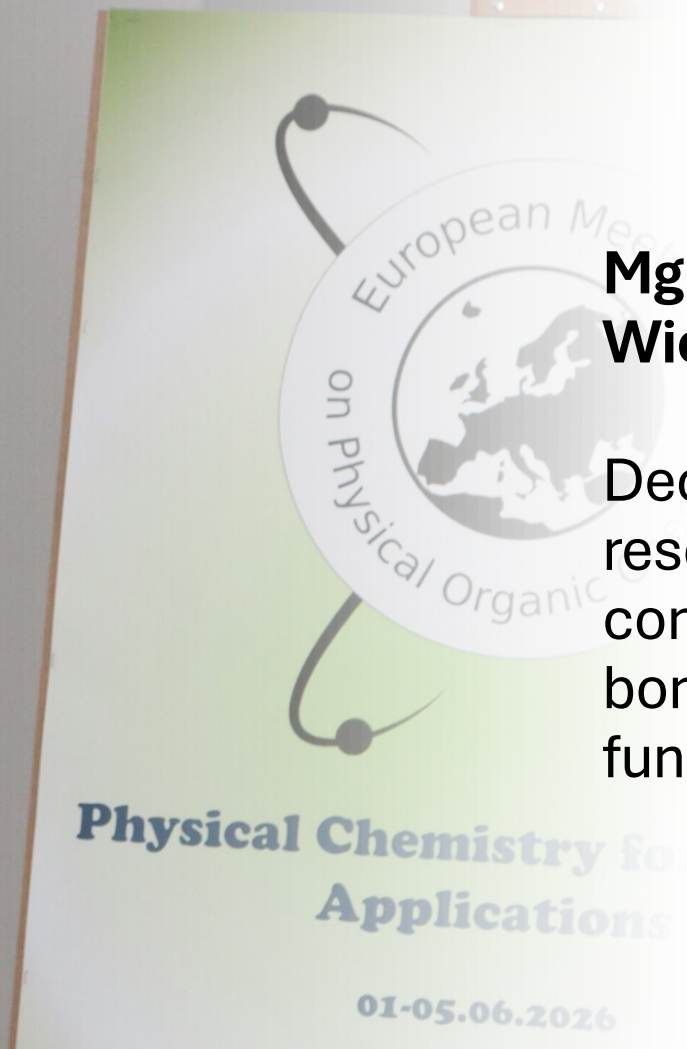
Machine learning in RNA
atomistic simulations



Dr hab. Dawid Dębowski, prof. UG

From molecular structure to
biological activity: Novel sulfonamide
derivatives





**Mgr Paweł
Wieczorkiewicz**

Decoding chemical
resonance in π -
conjugated systems with
bond delocalization
function (BDF)

Mgr Barbara Lech

Computational insights into the role
of 2-thiouracil in RNA self-
replication



Dr Kamil Wojtkowiak

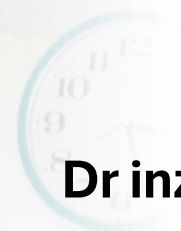
pH dependence of
protoribosomal RNA
conformational flexibility: MD
simulation parameters
benchmark and preliminary
results



Prof. dr hab. Piotr Cysewski

Solubility advantage of (natural) deep eutectic solvents: insight from measurements, quantum chemistry and machine learning





Dr inż. Karol Kułacz

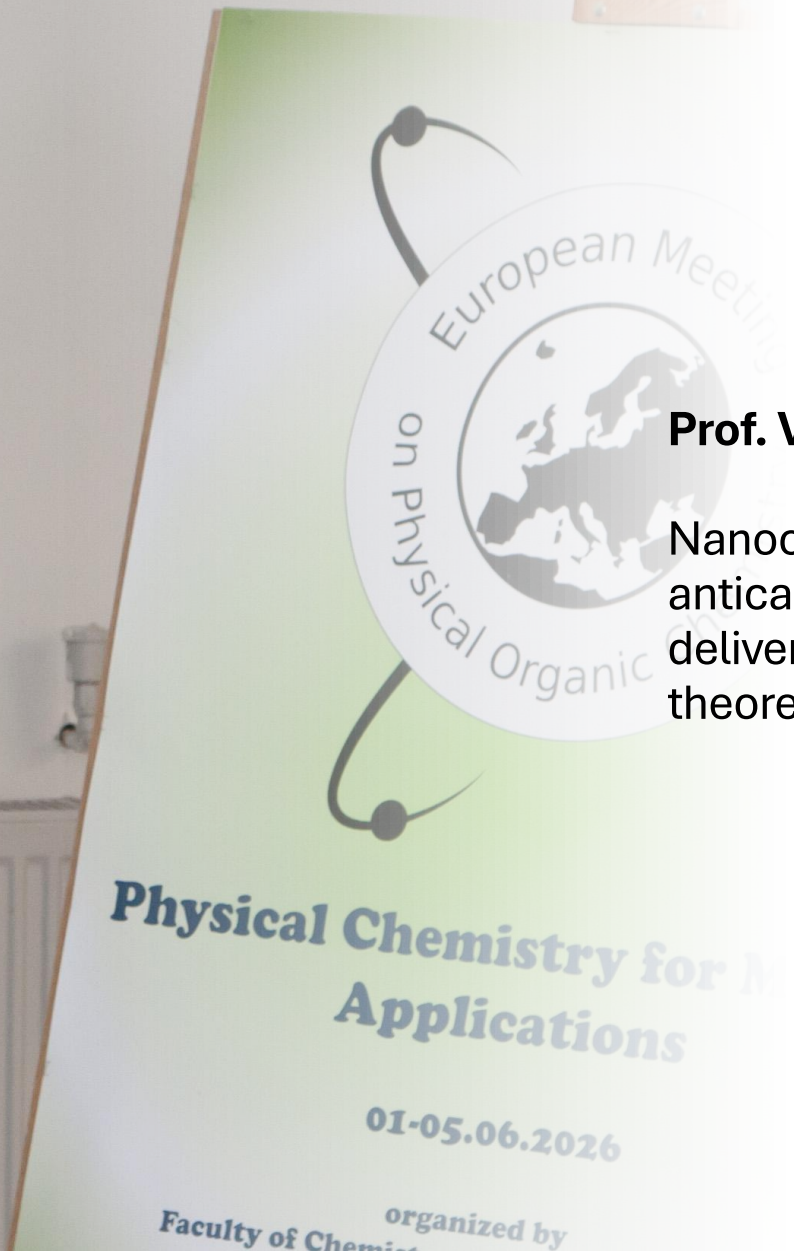
High temperature
deintercalation of DMSO
smectite

**Physical Chemistry for Medical
Applications**



Prof. Mirosław Jabłoński

A thorough Systematic conformational study of an experimentally known lantern-like superphane

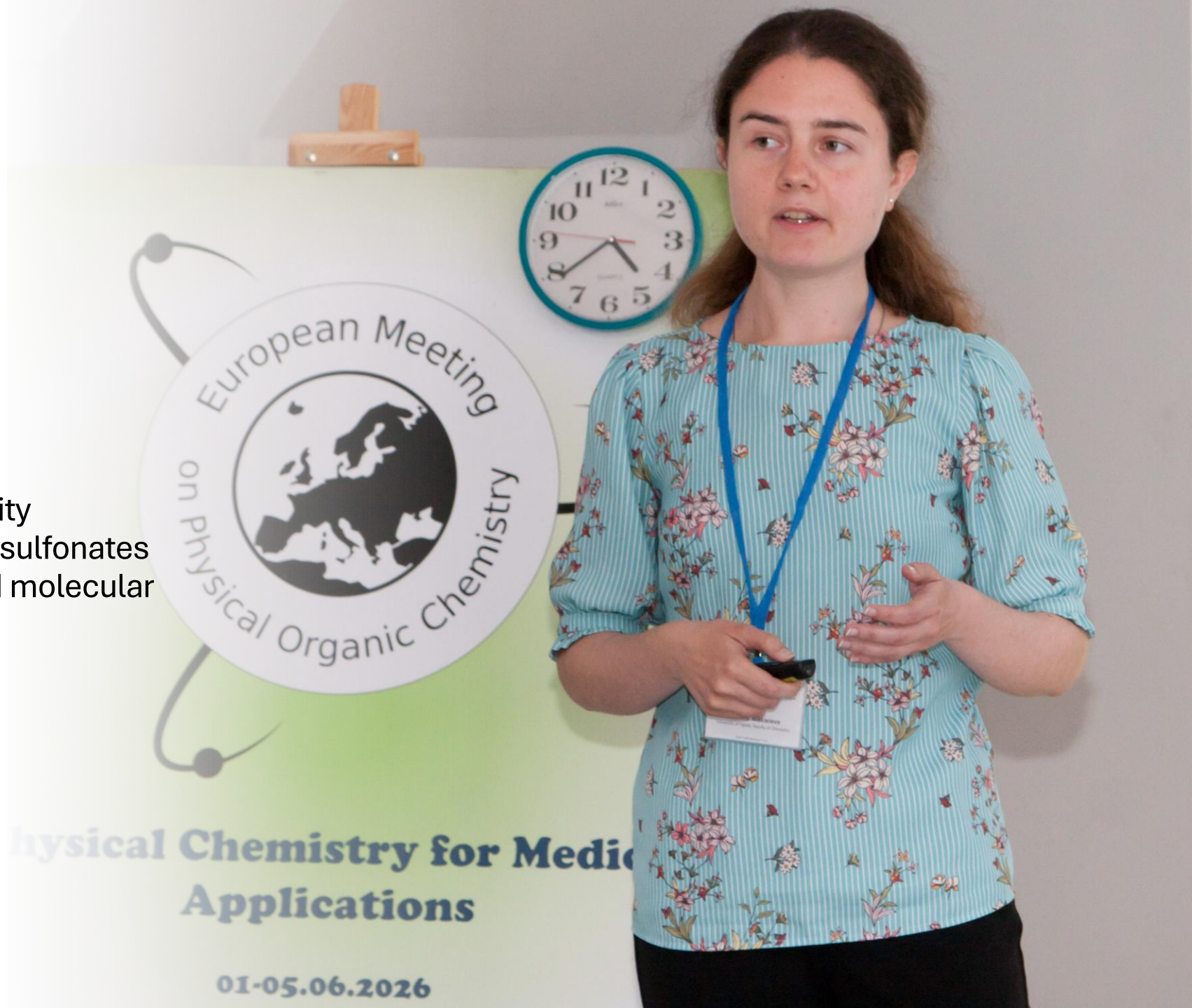


Prof. Vlada Pashynska

Nanocomposites of MoS₂ with anticancer drugs for drug delivery: experimental and theoretical characterization

Mgr Natalia Makieieva

Towards the structure-activity correlation for selected thiosulfonates - spectroscopic studies and molecular modelling



Mgr Patrycja Piękoś

Meso-benzodioxole-BODIPY as pH-sensitive fluorophores



Poster session



European Meeting
on Physical Organic Chemistry

**Physical Chemistry for Medical
Applications**


01-05.06.2026

organized by
Faculty of Chemistry, University of Wrocław
and
Section of Physical Organic Chemistry
of the Polish Chemical Society

<https://empoc.uwr.edu.pl/>







Politechnika
Wroclawska

Boluwatife B. Ogunnaiya, B.Sc.
Institute of Advanced Materials, Faculty of Chemistry,
boluwatife.ogunnaiya@pwr.edu.pl


Introduction

Nonenzymatic RNA replication predates protein enzymes and plays a fundamental role in the emergence of life [1]. Magnesium ions (Mg^{2+}) are essential to RNA function today and played a central role in stabilizing reactive intermediates and promoting bond formation [2,3]. In prebiotic chemistry, Mg^{2+} may have played a similarly critical role in facilitating the formation of phosphodiester bonds during template-directed RNA polymerization. Despite its significance, the precise catalytic contributions of Mg^{2+} in nonenzymatic RNA replication remain poorly understood. In this study, we employ molecular dynamics (MD) simulations to investigate how Mg^{2+} affects relevant RNA conformations; reactive geometry and base pairing stability across various systems, providing insight into potential catalytic configurations for early RNA self-replication.

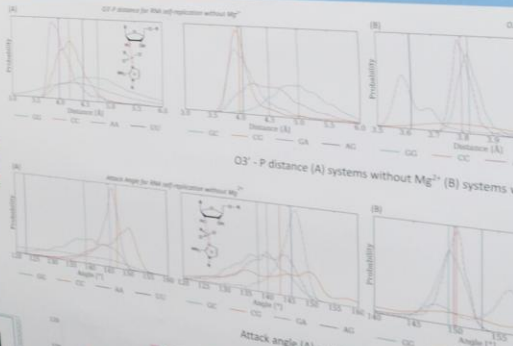
Computational details

Canonical RNA duplex systems with protonated phosphate backbones (with and without Mg^{2+}) and deprotonated backbones (with Mg^{2+}), across diverse sequence contexts: homologous (GG, CC, AA, UU), alternative (AA,UUU, UUU,AA, UU, UUCU), and heterogeneous (GC, CG, GA, AG). Each system consists of the template, 6 primer nucleotides, imidazole bridged dinucleotide intermediate, and 3 helper oligonucleotide. Using the Amber parmOL3 force field, each system was solvated in a truncated octahedral box (SPC/E water, 12 Å buffer) and neutralized with K^+ and Cl^- ions. Energy minimization and equilibration was performed. Three independent 500 ns MD simulations were conducted per system (300 K, 1 bar). Trajectories were clustered using DBSCAN and K-means to identify representative conformations for further analysis.

Results

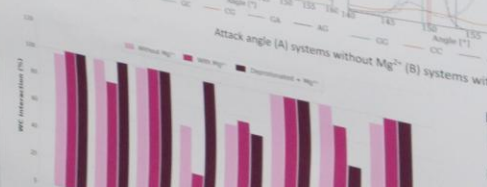


Labelled GC dinucleotide system




O3' - P distance (Å) systems without Mg^{2+} (A) systems with Mg^{2+} (B)

Attack angle [°] systems without Mg^{2+} (A) systems with Mg^{2+} (B)



Watson-Crick base pairing percentage across systems



Explore me

Conclusions

Mg^{2+} acts as a structural organizer for phosphodiester formation, narrowing attack-angle distributions and shortening $O3'-P$ distances, without necessarily improving Watson-Crick base-pair fidelity. Flexible dinucleotide intermediates such as UU can still achieve favourable geometries in the presence of Mg^{2+} , highlighting the importance of backbone organisation over base-pairing strength. Pyrimidine thiolation improves Watson-Crick base-pairing fidelity and enhances structural readiness for bond formation. The synergistic effect of thiolation and Mg^{2+} further improves the structural preorganization for nucleophilic attack. Overall, metal ions, nucleotide combinations, and chemical modifications work together to aid the self-replication mechanism of RNA. We believe that this study could have occurred in the prebiotic era.

References

- [1] Lech, B.K., Ogunnaiya, B. (2025) <https://doi.org/10.1039/d5cc00031a>
- [2] Mittal, S., Nisler, J., Szostak, J.P. (2014) <https://doi.org/10.1039/c4cc00031a>
- [3] O'Flaherty D.K., et al. (2014) <https://doi.org/10.1039/c4cc00031a>

This work has been supported by the National Science Foundation (NSF) grant number 1809303. This work was supported by computational resources from the EMPOC 01-05.06.2026

For WITaO Systems Witeszcz - 2026



Analysis of follicular fluid samples by FT-IR and NMR spectroscopy

Kamil Sobieszuk

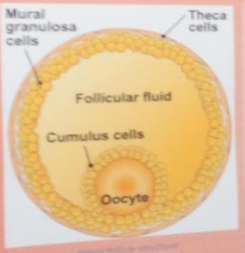
Faculty of Chemistry, University of Wrocław, 14 F. Joliot-Curie, 50-383 Wrocław, Poland

Abstract:

Infertility is defined as inability to conceive after a year of regular, unprotected sexual intercourse, with approximately 1 in 6 people globally experiencing it in their lifetime. However, the diagnostic process is lengthy and often requires several invasive procedures. For this reason, alternative protocols are being investigated, such as identifying infertility markers in biological fluids by spectroscopy.

This study focused on the analysis of follicular fluid of infertile and fertile women by FT-IR and NMR spectroscopy and identifying differences in their spectra, which in conjunction with medical data could be used in sample classification. The IR spectra were recorded using the ATR technique by applying 1 µl of liquid sample onto the ATR crystal and drying it under a steady nitrogen flow for 10 minutes, before collecting the data. In the case of NMR measurements, 30 µl of sample was mixed with phosphate buffer in deuterated water and 1D-NOESY sequence was applied.

The data was then analysed by PCA and PLS-DA with medical diagnostic information used for class assignment. Clear clustering of data points was observed, suggesting the presence of minute differences between the composition of follicular fluid in fertile and infertile women. This is supported by PLS-DA loadings showing the largest contributions to class separation as signals in the amide band region and 3600-2800 cm⁻¹ region which is comparable to the calculated difference spectrum between the mean spectra of both sample classes.



- Follicular fluid composition:**
- Gonadotropins - luteinizing hormone (LH) and follicle stimulating hormone (FSH)
 - Sex hormones - estradiol, progesterone & androgens
 - Anti-Müllerian hormone (AMH), inhibin and inhibin B
 - Proteins
 - Albumin globulin from plasma
 - Transferrin, IgG, IgM, IgA
 - Complement (C3, C4, C5, C6, TNF-α, IL-10)
 - Growth factors (IGFBP, IGF, IGF-1)
 - Amino acids
 - Lipids - phospholipids, triglycerides, cholesterol
 - Glucose
 - Lactate
 - Hippuronic acid
 - Extracellular vesicles

Experiment:

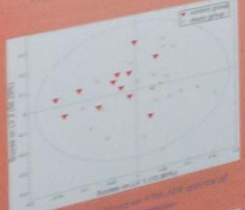
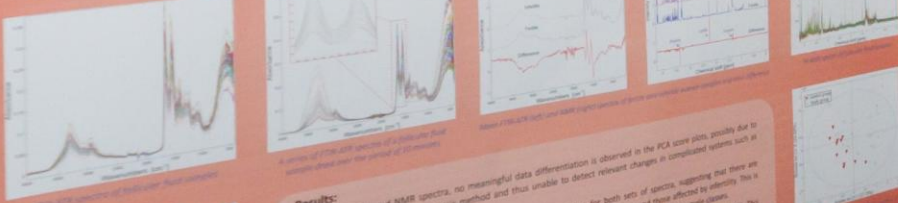
A series of 34 samples of follicular fluids from fertile and infertile women, was first analysed by FT-IR spectroscopy, specifically the attenuated total reflection (ATR) technique, using a Nicolet 550 FT-IR spectrometer (ThermoFisher) fitted with a GoldenGate ATR accessory (Spectra). The measurements were performed on dry film, with 1 µl of follicular fluid placed onto the ATR crystal and dried in the atmosphere of nitrogen gas for 10 minutes. The absorption spectra were recorded in the 4000-400 cm⁻¹ range at 4 cm⁻¹ resolution, averaging 128 scans.

Afterwards, the remaining 30 µl of FF samples were deproteinized by the addition of 250 µl of methanol, vortexed and centrifuged at 13400 g for 30 minutes. The supernatant was collected and the solvent evaporated. The obtained solid was subsequently dissolved in 540 µl of phosphate buffer with the addition of 60 µl of deuterated water with TMSF standard and 1D-NOESY proton spectra were recorded on a Bruker Avance spectrometer with a 600 MHz magnet and a Broadband Inverse (BB1) probe, averaging 64 scans, with a 600 MHz magnet and a Broadband Inverse (BB1) probe, averaging 64 scans.

The obtained ATR and NMR spectra were uploaded to MATLAB (ver. R2020b, MathWorks), transformed into data matrices and class vectors were created, based on the patients' fertility. The data was then analysed by principal component analysis (PCA) and partial least squares-discriminant analysis (PLS-DA) methods, utilizing the PLS_Toolbox (ver. 6.2, Eigenvector) software in the MATLAB environment.



FT-IR spectroscopy



Results:

For both ATR and NMR spectra, no meaningful data differentiation is observed in the PCA score plots, possibly due to being an unsupervised chemometric method and thus unable to detect relevant changes in complicated systems such as biological samples.

On the other hand, PLS-DA plots show clustering based on class for both sets of spectra, suggesting that there are detectable differences between the composition of follicular fluid of healthy women and those affected by infertility. This is supported by the PLS-DA loading plots resembling the difference spectrum between means of both sample classes.

Due to the FT-IR data differentiation being less pronounced, second derivative spectra were utilized using MATLAB. This drastically improved class differentiation, with no overlap between the clusters, suggesting that certain important variables in the ATR spectra are covered up by stronger vibrational modes of other molecules in the sample.



MR3/62



fot. Władysław Wizeszcz - 2026

CHEMICAL BRAIN FINGERPRINT OF A RAT WITH ASD-INDUCED DYSFUNCTION

Emilia Wrona^{1,2}, Anna Błasiak¹, Aleksandra Noga^{1,3}, Aleksandra Kurek¹, Aleksandra Woźniak-Brozyna¹

¹ Faculty of Chemistry, Jagiellonian University, 30-387 Kraków, Poland
² Doctoral School of Exact and Natural Sciences, Jagiellonian University, 30-048 Kraków, Poland
³ Department of Neurophysiology and Chronobiology, Institute of Zoology and Biomedical Research, Jagiellonian University, 30-387 Kraków, Poland

Introduction
 Autism spectrum disorders (ASD) are neurodevelopmental disorders that appear in fetuses and very young children. Changes associated with ASD have been observed in brain structures such as the midbrain, hippocampus and temporal and occipital lobes. Individuals diagnosed with ASD have difficulty with social interactions and may exhibit repetitive behaviors. The severity and frequency of symptoms vary from person to person, making both diagnosis and understanding the underlying mechanisms of the disorder a significant challenge. Currently, the diagnosis of ASD relies more on behavioral assessment than on structural changes in the brain.

The aim of the study
 The aim of the study was to check whether we could observe differences in the Raman spectroscopic image of the brain tissue of rats with induced ASD compared to healthy animals.

Experimental
 The study used horizontal brain sections obtained from animals with induced ASD. Sprague-Dawley rats were used. Prenatal exposure to valproic acid was used to induce ASD. Spectra were recorded using a Renishaw inVia Qontor spectrometer in the 3200-300 cm^{-1} range using a 785 nm laser line. An immersion objective (60x, NA=0.75) was used. To maintain constant temperature and humidity, an Okolab Cage Incubation system was used in combination with a CO₂-UNIT-BL device. Principal component analysis was performed using Unscrambler X software (version 10.3, Camo Software, Oslo, Norway).

Results
 PCA analysis confirmed that the differentiation of samples is primarily associated with changes in lipid and protein structure. In the first stage, the entire spectral range - 3200-300 cm^{-1} - was analyzed. The bands indicate changes in the organization of phospholipids or differences in the vibrations of lipid CH groups and the degree of order in cell membranes. Based on the spectra, smaller wavenumber ranges were selected and analyzed. Bands in the 1269-1245 cm^{-1} range are mainly associated with amide III vibrations and unsaturated lipids. Bands around 1330 cm^{-1} are associated with CH₂ and CH₃ scissoring vibrations. Changes in the 1220, and 1364 cm^{-1} regions are associated with vibrations originating from Tyr and Phe (for the 1208 and 1220 cm^{-1} bands) and Ser (for the 1364 cm^{-1} band). Bands around 1674-1631 cm^{-1} correspond mainly to amide I vibrations associated with protein conformational changes, whereas in the 1452-1438 cm^{-1} range, the changes are associated with CH₂ group vibrations of lipids. Differences between the groups are also visible in the 3200-2700 cm^{-1} range, in the CH vibration range.

- References**
- [1] Lamoreaux, J., et al. *PLoS One*, 2019, 14(12), e0224242.
 - [2] Mierzejewski, T., et al. *PLoS One*, 2020, 15(12), e0242424.
 - [3] Mierzejewski, T., et al. *PLoS One*, 2020, 15(12), e0242424.
 - [4] Mierzejewski, T., et al. *PLoS One*, 2020, 15(12), e0242424.
 - [5] Mierzejewski, T., et al. *PLoS One*, 2020, 15(12), e0242424.
 - [6] Mierzejewski, T., et al. *PLoS One*, 2020, 15(12), e0242424.
 - [7] Mierzejewski, T., et al. *PLoS One*, 2020, 15(12), e0242424.
 - [8] Mierzejewski, T., et al. *PLoS One*, 2020, 15(12), e0242424.
 - [9] Mierzejewski, T., et al. *PLoS One*, 2020, 15(12), e0242424.

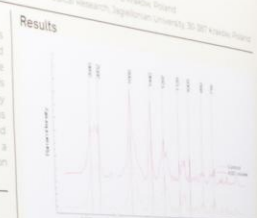


Fig. 1. Averaged Raman spectra for the examined brain area, obtained after excitation with a 785 nm laser for three populations of rats with autism spectrum disorder.



Fig. 2. Results of PCA analysis of Raman spectra for the brain regions. The comparison of data from the ASD model with data from healthy rats in the entire range (3200-300 cm^{-1}) and in smaller ranges: (a) 1269-1245 cm^{-1} , (b) 1330 cm^{-1} , (c) 1220-1208 cm^{-1} , (d) 1364 cm^{-1} .

Conclusion
 PCA analysis showed clear biochemical differences between the study groups, primarily related to changes in lipid conformation, the degree of cell membrane order, and protein conformation. In addition, a band originating from cholesterol appears at 1330 cm^{-1} and vibrations resulting from the presence of amino acids such as Tyr and Phe were observed. The results indicate that both structural changes in lipids and proteins contribute to the biochemical differentiation of the analyzed samples.

Acknowledgements
 The authors thank the National Science Centre (NCN) for the financial support of this project (grant number 2019/01/X/ST1/00001).





Association of Chemistry, F. Joliot-Curie 14, Wrocław, 50-383, Poland
334224@awr.edu.pl

Introduction

Menthol can form linear and cyclic associates. The strong electric field shifts equilibrium toward open associates of large dipole moments, that may result in noticeable NDE increment ($\Delta\epsilon$)

Linear associate: CC1=CC=C(C=C1)C(C)C
cyclic associate: CC1=CC=C(C=C1)C(C)C
Figure 1. Structures of associates in hydroxy alcohols.

The non-linear dielectric effect (NDE) is determined by measuring the difference in electric permittivity at strong and weak electric fields. [1] This difference is called the NDE increment ($\Delta\epsilon_{NDE}$). NDE measurements are typically performed for liquids, while measurements for solids are difficult and depend on size. [2]

According to the Debye-Caperson theory, a dipolar liquid the NDE increment should be negative and proportional to the square of the electric field strength. However, a strong response (to both to the appearance of a positive, so-called anomalous NDE increment, conventional theory, intermolecular association, critical fluctuations, and equilibrium phenomena). [3]

In this study we present dielectric, 1H -NMR, IR measurements and DFT calculations in a representative and menthol-1,4-dioxane system. The NDE measurements were performed at electric permittivity, density and refractive index data. In the course of experiment we compare the experimental NDE with calculated one in the frame of the Debye-Caperson theory.

Methods

Experiment of non-linear dielectric measurements

The experiment is based on comparison of the values of electric permittivity measured at high and at low electric field strength. Capacitor which contained the investigated liquid was a part of LC circuit. Resonance frequency allowed to calculate the permittivity with a resolution up to 10⁻⁵. LC circuit was operated at frequency of 4.1 MHz and low-amplitude of 1 V. For a short time (of 1 ms) a high voltage pulse was applied (500-3000 V) and the change of the resonance frequency of LC circuit caused by the change of electric permittivity was measured. This allowed to calculate the NDE effect expressed as $\Delta\epsilon_{NDE}/E^2$, where $\Delta\epsilon_{NDE}$ is the difference between electric permittivity obtained at high electric field strength and at low electric field strength. Details of experimental setup can be found in paper. [5]

Experiment of linear dielectric measurements

Measurements of electric permittivity were performed using HP 4284A Precision LCR Meter (frequency range 100 Hz - 1 MHz). Capacitor had coaxial configuration. Geometry capacity and capacity was obtained using liquids of known permittivity (air, 1,2-dichloroethane). Geometric capacitance was found of 5 pF. Temperature was stabilized by water thermostat at 25 ± 0.1 °C. Measurements in the frequency range 1 MHz - 4 GHz were performed using the Copernicus VNA analyzer. The sample was located at the end of the coaxial line.

XRD Experiment

Diffraction data were collected at 100 K using CuK α radiation on a Xcalibur Ruby (Rigaku) Diffraction single-crystal diffractometer. Data reduction was performed in CrysAlisPro [6], structures were solved with SHELXS/SHELXT [7, 8] and refined by full-matrix least squares. Non-hydrogen atoms were refined anisotropically, while hydrogen atoms were located from difference electron density maps.

Results

menthol-p-xylene

menthol-1,4-dioxane

Discussion and conclusions

The results of the experiment show that the NDE effect is negative, but at more than 10⁶ V/m it becomes positive. This effect is likely due to the formation of linear-polar molecular associates (monomers) and cyclic associates (trimers/tetramers, of a possible structure shown in Figure 1). XRD analysis revealed a three-leaf clover-like motif formed by

for: Władysław Wzieszczył 2026



INTRODUCTION

Erythrocytes are specialized cells responsible for transporting oxygen and carbon dioxide through hemoglobin. Red blood cells undergo numerous biochemical and structural alterations that can serve as important indicators of overall health status [1, 2].

AIM

The aim of the study was to develop a spectroscopic profile of erythrocytes taking into account gender and age.

RESULTS & DISCUSSION

AVERAGE SPECTRA FOR 785 NM LASER LINE (COMPARISON OF WOMEN AND MEN)

Bands [cm ⁻¹]	Assignment
862	H-Hb ₁ , VC-CIP
1004	Trp ⁺
1121	Heme ν_2
1216	Bands IP ⁺
1462	Heme ν_2 , N(CH ₂ CH ₂) ⁺
1627	Amino IP ⁺
174	Heme ν_1
300	Heme ν_1
1010	Heme ν_2 , N(CH ₂ CH ₂) ⁺

PCA analysis comparison of old and young men, 3200–300 cm⁻¹, 785 nm laser. Clear distinctions between old and young men are observed with respect to PC-4. The table presents the bands and their assignments that have the greatest impact on spectral differentiation.

Bands [cm ⁻¹]	Assignment	Bands [cm ⁻¹]	Assignment
860	Young	740	Old
1233	Young	971	Heme ν_2
1623	Young	1423	Trp ⁺
		1501	Gln, v(CN) ⁺
		1501	Trp, Trp ⁺

AVERAGE SPECTRA FOR 514.5 NM LASER LINE (COMPARISON OF WOMEN AND MEN)

PCA analysis comparison of women and men, range 3200–300 cm⁻¹, 514.5 nm laser. A clear distinction between women and men with respect to PC-3. The bands and their assignments that have the greatest influence on differentiating the spectrum of red blood cells in women and men are presented in the table.

Bands [cm ⁻¹]	Assignment
300	Young
1240	Heme ν_2
1336	Heme ν_2
2020	Amino IP ⁺
	Leu ⁺ , PC, Heme ⁺
1040	Assignment
1292	Assignment
1540	Assignment
2832	Assignment

PCA ANALYSIS OF OLD AND YOUNG MEN, 785 NM LASER LINE

PCA analysis comparison of old and young men, 3200–300 cm⁻¹, 785 nm laser. Clear distinctions between old and young men are observed with respect to PC-4. The table presents the bands and their assignments that have the greatest impact on spectral differentiation.

Bands [cm ⁻¹]	Assignment	Bands [cm ⁻¹]	Assignment
860	Young	740	Old
1233	Young	971	Heme ν_2
1623	Young	1423	Trp ⁺
		1501	Gln, v(CN) ⁺
		1501	Trp, Trp ⁺

PCA ANALYSIS OF OLD AND YOUNG WOMEN, 514.5 NM LASER LINE

Bands [cm ⁻¹]	Assignment
300	Young
1240	Heme ν_2
1336	Heme ν_2
2020	Amino IP ⁺
	Leu ⁺ , PC, Heme ⁺
1040	Assignment
1292	Assignment
1540	Assignment
2832	Assignment

CONCLUSIONS

The results of the study showed that it is possible to distinguish between the gender and age of the subjects using Raman spectroscopy in combination with PCA analysis. Additionally, an analysis of the morphological parameters of erythrocytes (RBC) and hemoglobin concentration (HGB), as well as platelet count (PLT) [5].

STANDARD MEDICAL TESTS

Morphological parameters of erythrocytes (RBC) and hemoglobin concentration (HGB), as well as platelet count (PLT) [5].

Parameter	Value
Hemoglobin concentration	12.5
Red blood cell count	4.47
Platelet count	5.28

REFERENCES

[1] ... [2] ... [3] ... [4] ... [5] ...

Disorder to Stability: Modulation of Phytosterol-Containing DPPC Membranes

K. Masiał¹, A. Berce², K. Cieślak-Boczuła¹, A. Grygier², M. Rutńska³
¹Faculty of Food Science and Nutrition, Wrocław University of Life Sciences, Wrocław, Poland
²Faculty of Chemistry, Wrocław University of Science and Technology, Wrocław, Poland
³Faculty of Food Science and Nutrition, Wrocław University of Life Sciences, Wrocław, Poland



Introduction

Phospholipid based liposomes are widely used biomimetic models for investigating the structure and behavior of biological membranes. Their biocompatibility and ability to encapsulate both hydrophilic and hydrophobic compounds make them effective nanocarriers in drug delivery and nutraceutical applications. Among phospholipids, dimyristoylphosphatidylcholine (DMPC) is preferred for extending membrane modifications. Phytosterols, including stigmasterol and its fatty acid esters (stigmasterol stearate, palmitate), are cholesterol analogs that modulate bilayer properties such as fluidity and thermodynamic stability. However, their bulky structure can disrupt lipid packing and reduce phase transition cooperativity. To reduce these effects and improve liposome functionality, PEGylation is often applied which enhances colloidal stability, reduces immune recognition and prolongs circulation. This approach supports the formation of long-circulating liposomes with favorable pharmacokinetics and improved structural integrity.

Materials and methods

Liposome Preparation: Thin-film hydration with DPPC + phytosterols + DSPE-PEG2000
Spectroscopic Analysis: FT-IR spectra collected across 10-40 °C, 1.28 scans per sample at 2 cm⁻¹ resolution
PCA: Conducted in MATLAB R2019a to identify transition points and spectral clustering
TEM: Used to assess morphology and lamellarity

Thermotropic Shift



Sterols and esters

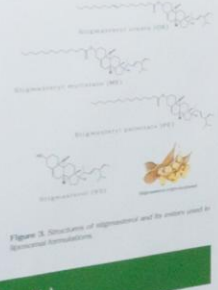


Figure 3. Structures of stigmasterol and its esters used in liposomal formulations.

Phase Transition Temperature (T_m)



Figure 4. Comparison of main phase transition temperature (T_m) for DPPC-based liposomes with and without PEGylation. The incorporation of DSPE-PEG2000 consistently elevated T_m across all tested systems (with the exception of those containing stigmasterol, where the transition was less pronounced), indicating a preventing process in demyelination, indicating a notable enhancement of the thermotropic stability and structural resilience of the lipid membrane environments.

PCA Analysis



Figure 5. FT-IR spectra and PCA analysis. The top part shows FT-IR spectra of DPPC-based liposomes at different temperatures. The bottom part shows PCA analysis results, including a score plot and a loading plot, highlighting the spectral differences between the formulations.

Liposome preparation

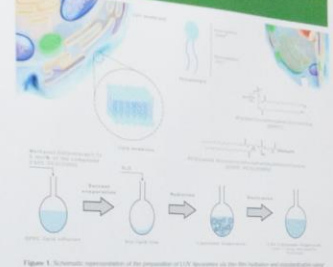


Figure 4. Schematic representation of the preparation of liposomes as the bilayer and distribution using DPPC and PEG2000.

Morphology

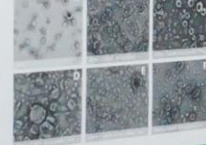


Figure 5. Transmission electron microscopy (TEM) images of liposomes under different conditions. The images show the morphology of liposomes, illustrating their spherical structure and size distribution.

Chain Conformation

Table 1. Summary of membrane properties (lipid composition, transition temperatures, and T_m) for DPPC-based liposomes with and without PEGylation.

Formulation	Transition Temperature (T _m) [°C]
DPPC	~35
DPPC + Stig	~38
DPPC + Stig + DSPE-PEG2000	~42
DPPC + Stig + DSPE-PEG2000 + PEG	~45

Shifts toward higher wavenumbers at elevated temperatures and in PEGylated systems indicate increased hydration, chain disorder, and substantial enhancement of membrane fluidity, reflecting a transition toward a more dynamic and less ordered lipid bilayer environment.

Cooperativity



Figure 7. Plot of cooperativity (C) versus temperature (T) for DPPC-based liposomes. The plot shows a sharp increase in cooperativity at the phase transition temperature, indicating a more cooperative transition in the PEGylated systems.

Conclusions

- PEGylation = Stabilization
- FT-IR + PCA = Insight
- Suppressing Disorder
- Toward Smart Nanocarriers








foto: Władysław Wizeszcz - 2026

Diagnosis of rheumatic diseases using vibrational spectroscopy and NMR-based metabolomics
 Department of Chemistry, University of Wrocław, Wrocław, Poland
 e-mail: przemyslaw.cugrych@uwr.edu.pl

Rheumatoid and psoriatic arthritis



Rheumatoid arthritis (RA) and psoriatic arthritis (PsA) are chronic autoimmune conditions that mainly target the musculoskeletal system. During the acute phase of both diseases, a variety of extra-articular lesions can affect several vital organs. RA is marked by symmetrical joint inflammation, especially of the small joints of the hands and feet, and erosion of bone at the base and periphery of the metacarpals. Psoriatic arthritis typically involves inflammation of the joints, as well as the tendons with the characteristic aspect of the disease, and also prominent features. Diagnosing RA and PsA remains challenging due to their similar characteristics and the absence of specific markers. Diagnosis typically relies on patient history, measurement of markers such as CRP and ESR, and imaging techniques like X-rays and ultrasonics. For RA, the ACR/EULAR criteria are used, while the CASPAR guidelines apply to PsA [1].

Donors

Patients with RA (n=34) and PsA (n=27) were recruited for the study at the Wrocław Medical University. The control group (C) consisted of 17 volunteers, selected based on comparable age and gender. Written informed consent was obtained from all volunteers, which was approved by the Bioethics Committee at Wrocław Medical University No. KB-159/2022) and was conducted in accordance with the guidelines of the Second Declaration of Helsinki. Patients with psoriatic arthritis with RA who were included in the study met the 2010 ACR/EULAR classification criteria. Patients with psoriatic arthritis with RA who were included in the study met the 2010 ACR/EULAR classification criteria. For the collected blood sera samples set of biochemical parameters was determined.

Spectroscopic conditions

Vibrational spectra of the biological material were collected using an 850 FTIR spectrometer. Raw data were obtained using FT-Raman accessory equipped a CaF_2 beam splitter and Nd:YVO₄ laser, emitting 1984 nm line, with a power of 150 mW at sample. Interferograms were illuminated using an Nd:YVO₄ laser, emitting 1984 nm line, with a power of 150 mW at sample. Interferograms were averaged over 512 scans, they were Happ-Genzel deconvoluted and Fourier transformed to spectra in the 100–2000 cm^{-1} range with a resolution of 8 cm^{-1} . NIR spectra were measured in Kubelka-Munk mode using a diffuse-reflectance optical assembly. A CaF_2 beam splitter and DTGS detector were used. Spectra of the lyophilizates were obtained by summing 64 scans. The interferograms were converted into spectra by protein precipitation, dissolved in a phosphate buffer at pH = 7.4, and D₂O standard solution of TMSP-d₄ was added. Measurements were performed using Bruker Avance II 600 MHz NMR spectrometer equipped with a BBO probe at 300K. 1D NOESY spectra with water presaturation were obtained by summing 64 scans.

Data treatment

Spectral data were transformed into MDS. All environment Raman spectra were combined using standard normal variate (SNV) technique. The second derivative of IR spectra were obtained using the Savitzky-Golay filter applying 15 data points and 3rd order polynomial. Before recording of spectra data were normalized. The PLS regression model was constructed of PLS-DA models was carried out using the PLS toolbox. The PLS regression model was constructed of PLS-DA models was carried out using the PLS toolbox. The PLS regression model was constructed of PLS-DA models was carried out using the PLS toolbox. The PLS regression model was constructed of PLS-DA models was carried out using the PLS toolbox.

Results

Collected vibrational spectra were used to train and validate a number of PLS-DA and CP-DA models. In the course of PLS-DA modeling, 1000 samples were divided into training and test sets. The PLS-DA models were trained using the training set and validated using the test set. The PLS-DA models were trained using the training set and validated using the test set. The PLS-DA models were trained using the training set and validated using the test set.

Conclusions

Vibrational and NMR spectra were a valuable source of information for the diagnosis of rheumatic diseases. The combination of vibrational spectroscopy and NMR-based metabolomics is a promising approach for the diagnosis of rheumatic diseases. The combination of vibrational spectroscopy and NMR-based metabolomics is a promising approach for the diagnosis of rheumatic diseases.



fot. Władysław Wrzeszcz - 2026

Conference deliberations

A row of white, modern conference chairs with horizontal stitching on the backrests, arranged along a long, dark conference table. The chairs are in a meeting room with a large window in the background, creating a bright, slightly blurred background with bokeh light effects.

















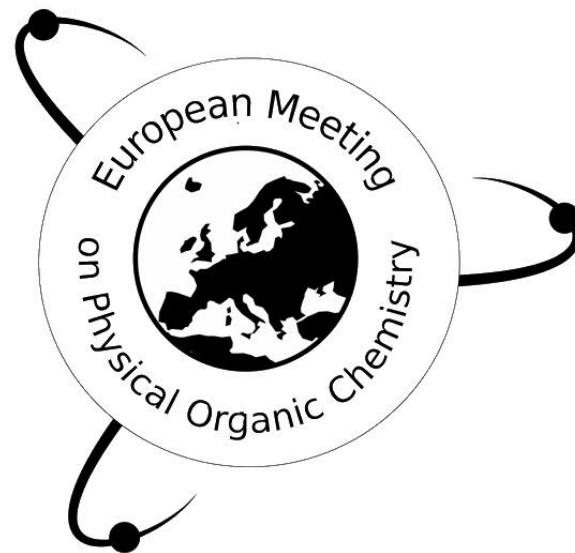












The next European Meeting on Physical Organic Chemistry will be held in June 2027.



We warmly invite you to participate and look forward to welcoming you.